International Journal of Microwave and Wireless Technologies, 2017, 9(6), 1339–1343. © Cambridge University Press and the European Microwave Association, 2017
doi:10.1017/S1759078717000757

RESEARCH PAPER

Recognition of jet engines via sparse decomposition of ISAR images using a waveguide scattering model

SIMON WAGNER[1] AND JOACHIM ENDER[1,2]

Air target recognition is a critical step in the radar processing chain and reliable features are necessary to make a decision. The number and position of jet engines are useful features to perform a pre-classification and give a list of possible targets. To extract these features, a sparse decomposition framework for inverse synthetic aperture radar (ISAR) images is presented. With this framework different components of the target can be detected, if signal models for these parts are available. To use it for the detection of jet engines, a review of a signal model for air intakes, which was developed by Borden, is given. This model is based on the common assumption that the propagation of electromagnetic waves inside jet engines has the same dispersive behavior as inside waveguides. With this model a decomposition of a real ISAR image, measured with the tracking and imaging radar system of Fraunhofer FHR, into point-like scattering centers and jet engines is presented.

Keywords: Radar applications, Radar signal processing and system modeling, Waveguide scattering

Received 14 October 2016; Revised 23 June 2017; Accepted 23 June 2017; first published online 24 July 2017

I. INTRODUCTION

In the field of non-cooperative target recognition with radar, several different techniques have been introduced for the classification of air targets. All of these techniques extract information from the scattered signal, like micro Doppler modulations from moving parts, especially jet engine modulation (JEM) produced by the fan or compressor of the engine [1]. Other techniques, like high-resolution range profiles [2, 3] or inverse synthetic aperture radar (ISAR) [1, 4], exploit the imaging capabilities of radar. For these techniques a waveform with a high bandwidth, like a linearly frequency modulated (LFM) chirp, is necessary [5]. Most of the high-resolution-based classifiers are trained on a limited amount of similar targets and are used to distinguish between them. This procedure is based on the assumption that the class such as airliner, business jet, fighter or transport aircraft can be discriminated by a previously applied classifier.

This paper is an extension of [6] and a technique, which can be used as part of a pre-classification stage to eliminate a huge number of potential targets, is presented. With the proposed decomposition of ISAR images, the number and position of jet engines of targets visible in ISAR images can be determined. With these features a separation of targets with wing- and fuselage-mounted engines is possible, further is the number of engines significant for a list of possible targets used for the final classification [7]. The efforts presented in the past to locate jet engines in ISAR images are based on the Doppler spread and the resulting JEM lines. In [8], range-Doppler signatures with short dwell times were used to detect jet engines along the target. In [9], an algorithm to detect the range position of jet engines in ISAR images was introduced that utilizes the occurring JEM lines. A drawback of both given examples is that only the range position of the jet engines can be determined with these methods. With the method proposed here also the cross range position and the number of engines can be extracted.

For the feature extraction, a sparse decomposition of the ISAR image is performed. To achieve a separation between engine scatterers and normal scattering centers, two different signal models are necessary to form the dictionary for the sparse decomposition. As signal model for the normal scattering centers, the common isotropic point scattering model is used. For the engine scattering, a waveguide scattering model, which is very common to model jet engines [10] is utilized. This model describes a dispersive behavior of the cavity of the engine, such that the LFM chirp is extended in time and produces artifacts in the image. For these artifacts, a mathematical description that is used as model for the decomposition algorithm was introduced by Borden [11]. Both models are reviewed in Section II and the sparse decomposition framework is presented in Section III. An example of the decomposition applied to a real ISAR image, measured with the tracking and imaging radar (TIRA) of Fraunhofer FHR, is shown in Section IV. Finally, Section V concludes the paper and points out some open problems for future research.

[1]Fraunhofer Institute for High Frequency Physics and Radar Techniques, Wachtberg, Germany.
[2]Center for Sensorsystems, University of Siegen, Siegen, Germany
Corresponding author:
S. Wagner
Phone: +49 228 9435 365
Email: simon.wagner@fhr.fraunhofer.de

https://doi.org/10.1017/S1759078717000757 Published online by Cambridge University Press

II. ISOTROPIC AND WAVEGUIDE SCATTERING SIGNAL MODELS

For the proposed framework two distinguishable signal models of jet engines and point targets are necessary. The general idea of the engine model is to model the entrance structure as a circular terminated waveguide. Within this model the scattered field $\vec{E}^S$ of the jet engines can be considered as a sum of three independent parts, which are depicted in Fig. 1. These scattering mechanisms are a strong reflection $\vec{E}^S_{rim}$ from the edge at the opening of the engine, weak reflections $\vec{E}^S_{ext}$ from the exterior of the engine and the reflection $\vec{E}^S_{wg}$ from the fan or the first stage of the compressor inside the engine [12]

$$\vec{E}^S = \vec{E}^S_{rim} + \vec{E}^S_{ext} + \vec{E}^S_{wg}. \tag{1}$$

The first two elements of the sum are non-dispersive and can be modeled as common isotropic frequency-independent scatterers. With y as the range and x as the cross-range direction this model is written as

$$s_p(k_x,\ k_y,\ x,\ y) = e^{-j2(k_x x + k_y y)}, \tag{2}$$

which is used to describe a scattering center in the two-dimensional (2D) k-space domain [5]. k_x and k_y are the wavenumbers in there specific directions, calculated with the small aperture approximation by $k_x = k\sin(\Theta) \approx k\Theta$ and $k_y = k\cos(\Theta) \approx k$, where Θ is the azimuth angle of the target and k is the wavenumber of the transmitted instantaneous frequency. With a band-limited 2D inverse Fourier transform we get the point spread function (PSF) in the image domain, a 2D sinc-function

$$\begin{aligned} PSF_p(x', y') &= \iint_{\mathbb{K}} e^{-j2(k_x x + k_y y)} e^{j2(k_x x' + k_y y')} dk_x dk_y \\ &\approx A \cdot \mathrm{sinc}(\bar{k}\Delta\Theta(x' - x))\,\mathrm{sinc}(\Delta k(y' - y)), \end{aligned} \tag{3}$$

which will be used in the dictionary for the standard scatterer at position (x',y'). The inverse Fourier transform is band-limited because the covered area $\mathbb{K}$ of k_x and k_y is limited. $\Delta\Theta$ is the totally covered aperture during the imaging process, Δk is the used bandwidth in k-space $k_{\max} - k_{\min}$ and $\bar{k} = (k_{\min} + k_{\max})/2$. The complex scaling factor A can be ignored in the proposed framework, since this is working on the magnitude image and uses normalized PSFs. An example of the PSF, weighted with a Hamming window, is shown in Fig. 3(a).

Inside a waveguide, the propagation speed of the electromagnetic wave depends on the frequency, which is called *waveguide dispersion*. This dispersion will spread the transmitted LFM waveform in time and thus the pulse compression, which is fitted to a certain pulse length, will lead to delayed returns in the received signal. These *duct delayed returns* produce artifacts in the range direction of the image behind the physical position of the waveguide structure. An example of these delayed returns is depicted in Fig. 2(a), which is a nose on ISAR image of a small business jet. The duct delayed returns can be seen behind the engines, of which the position is visible in the target shape in Fig. 2(b).

To model this waveguide effect, the standard model s_p in (2) must be corrected with a dispersion term including a wavenumber k_y in range, which is nonlinearly dependent on the frequency ω

$$s_{wg}(k_y, L, \omega) = e^{-j2Lk_y(\omega)}. \tag{4}$$

This term represents the propagation of the incident wave to the terminated end of the waveguide over its length L and back. The general form of the wavenumber in dispersive media is given by [13]

$$k(\omega) = \frac{-j}{c_0}\sqrt{j\omega + a + b}\sqrt{j\omega + a - b}. \tag{5}$$

The appropriate choice of a and b in a hollow metallic waveguide are $a = 0$ and $b = j\omega_c$, which is the cut-off frequency of the propagating mode. With this substitution, (5) results in

$$k_{wg}(\omega) = \frac{1}{c_0}\sqrt{\omega^2 - \omega_c^2}. \tag{6}$$

Using (6) as $k_y(\omega)$ in (4), the corrective term becomes

$$s_{wg}(k_y, L, d) = e^{-j2L\sqrt{k_y^2 - \kappa_m^2}}, \tag{7}$$

where κ_m is the cut-off wavenumber of the mode m. It is known from electromagnetic theory that inside waveguides electromagnetic waves propagate in discrete modes κ_m, which depend on the diameter d of the opening [13]. Thus,

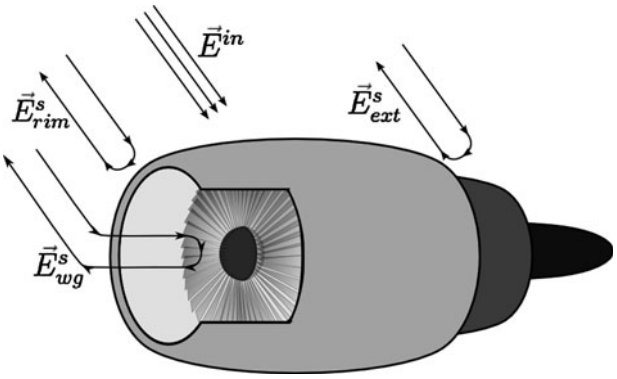

Fig. 1. Different scattering mechanisms of a jet engine.

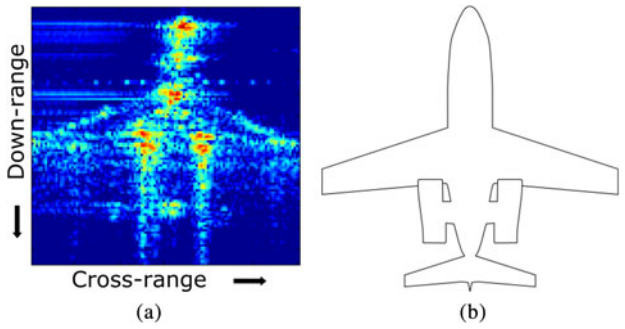

Fig. 2. Image and shape of the target. (a) Testimage, (b) shape of the target.

https://doi.org/10.1017/S1759078717000757 Published online by Cambridge University Press

(7) must be replaced by a sum over the propagating modes if an inlet is located at the corresponding position [14],

$$s_{wg}(k_y, \Theta, L, d) = \frac{1}{k_y}\sum_{m=1}^{M} S_m(\Theta, k_y) e^{-j2L\sqrt{k_y^2-\kappa_m^2}}. \quad (8)$$

The term $S_m(\Theta, k)$ in (8) represents the energy spread of the waveform. Since the opening of the engine is large compared with the wavelength of the radar, many modes will propagate inside the waveguide and the energy of the waveform is spread over them. The number of modes M is limited by the largest transmitted frequency $k_{\max}$,

$$M = \max\{m|\kappa_m \le k_{\max}\}. \quad (9)$$

To calculate the PSF of a waveguide scatterer, the inverse Fourier transformation of the corrected range term with the standard model in cross-range must be determined, which leads to [11]

$$PSF(x,y) \approx \underbrace{\operatorname{sinc}(\bar{k}\Delta\Theta x)}_{PSF_x} \underbrace{\sum_{m=1}^{M} S_m \int_{2k_{\min}}^{2k_{\max}} \frac{1}{k_y} e^{-j2L\sqrt{k_y^2-\kappa_m^2}} e^{jk_y y} dk_y}_{PSF_y}. \quad (10)$$

Equation (10) is a multiplication of two separated imaging kernels in the x- and in the y-direction. The kernel in the x-direction only depends on the carrier frequency $\bar{k}$ and the complete rotation angle $\Delta\Theta$ of the target and is the same as for the standard signal model. The kernel in range direction is a weighted sum of integrals, that still has to be examined and for a more detailed version of the following deviation of the PSF, the reader is referred to the original paper of Borden [11] or his textbook [14]. The first step is the substitution

$$e^{-j2L\sqrt{k_y^2-\kappa_m^2}} = 2j\sqrt{k_y^2-\kappa_m^2}\int_L^\infty J_0\left(2\kappa_m\sqrt{y'^2-L^2}\right)e^{-j2k_y y'}dy', \quad (11)$$

where $J_0(\cdot)$ is the Bessel function of the first kind. With this substitution and a rearrangement of k_y, the integral in (10) can be written as

$$2j\int_L^\infty J_0\left(2\kappa_m\sqrt{y'^2-L^2}\right) \times \int_{2\max(k_{\min},\kappa_m)}^{2k_{\max}} \sqrt{1-\left(\frac{\kappa_m}{k_y}\right)^2} e^{j2k_y(y-y')}dk_y dy', \quad (12)$$

where the lower bound of the initial integral in (10) is changed since components below the cut-off frequency of the specific mode will be exponentially damped. The expression in (12) can be interpreted as a convolution of the Bessel function with the second integral, which can be approximated as

$$\int_{2\max(k_{\min},\kappa_m)}^{2k_{\max}} \sqrt{1-\left(\frac{\kappa_m}{k_y}\right)^2} e^{j2k_y(y-y')}dk_y \approx \alpha\Delta k_{(1,c)}\operatorname{sinc}\left(\Delta k_{(1,c)}(y-y')\right)e^{j2\bar{k}_{(1,c)}(y-y')}. \quad (13)$$

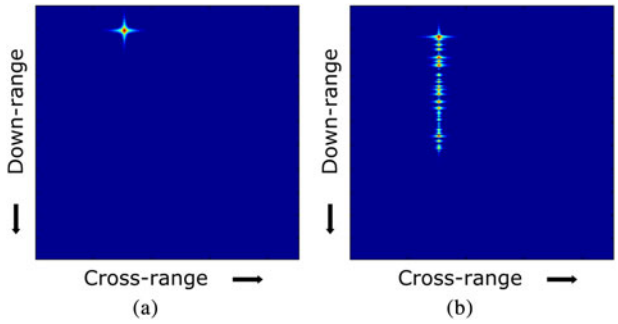

Fig. 3. Point spread functions for different scattering mechanisms. (a) PSF point scatterer, (b) PSF waveguide scatterer.

In (13), the width of the sinc-function depends on the bandwidth of this specific mode, which is defined as $\Delta k_{(1,c)} = k_{\max} - \max(k_{\min}, \kappa_m)$. $\bar{k}_{(1,c)}$ is the center frequency of the mode defined as $(\max(k_{\min}, \kappa_m) + k_{\max})/2$. With these definitions the final version of the imaging kernel in range direction is

$$PSF_y = \sum_{m=1}^{M} 2jS_m\alpha\Delta k_{(1,c)}\int_L^\infty J_0\left(2\kappa_m\sqrt{y'^2-L^2}\right)\cdots \times \operatorname{sinc}(\Delta k_{(1,c)}(y-y'))e^{j2\bar{k}_{(1,c)}(y-y')}dy'. \quad (14)$$

From (14) it is visible that the down-range effect in the image domain has the form of the function $J_0(y)$, shifted according to $y \to \sqrt{y^2-L^2}$ dilated by $y \to 2\kappa_m y$ and blurred by the $\operatorname{sinc}(\Delta k_{(1,c)}(y-y'))$ function. In this first approach the amplitudes S_m are given by $1/m$ and the energy of the PSF is normalized to one.

A point not considered by this model is the length of the artifacts in the ISAR image. Since the Bessel function is damped with a factor of $y^{-1/2}$ for large y, the tail would be visible over the complete image, if the image is depicted in an appropriate dynamic range in dB. In the example of Fig. 2(a), it can be seen that the damping is much stronger than the term of the Bessel function. Because of this, the Bessel function is truncated after a certain reasonable length. An example of a 2D waveguide PSF is depicted in Fig. 3(b).

III. SPARSE DECOMPOSITION FRAMEWORK

The sparse decomposition framework is based on the assumption that the ISAR image $I(x, y)$ under test can be represented as a sum of an Image $I_p(x, y)$ with point-like scatterers and an image $I_{wg}(x, y)$ with waveguide scatterers,

$$I(x,y) = I_p(x,y) + I_{wg}(x,y). \quad (15)$$

This framework is closely related to the one in [15], where SAR images were decomposed in clutter and target content by a technique called morphological component analysis [16]. To separate the image in the two components, a so called *dictionary* Φ is needed for each of the components. These dictionaries must represent the corresponding content sparsely and should be inefficient to represent contents of the other component. In the proposed framework, the

https://doi.org/10.1017/S1759078717000757 Published online by Cambridge University Press

dictionaries contain the different PSFs of point-like and waveguide scatterers at all possible positions in the image. In the literature on sparse representation, the single functions of the dictionary are called *atoms*. With these dictionaries both components can be described by a matrix vector multiplication of the dictionary with a corresponding coefficient vector, α:

$$I_p(x, y) = \Phi_p \alpha_p, \tag{16}$$

$$I_{wg}(x, y) = \Phi_{wg} \alpha_{wg}. \tag{17}$$

To form the dictionaries in (16) and (17) the 2D PSFs are vectorized into 1D vectors. Thus the images I_p and I_{wg}, marked in the equations as 2D, are also 1D vectors. For the following description of the algorithm, the so-called l_p-norm

$$||x||_p = \left(\sum_{i=1}^{N} |x_i|^p \right)^{1/p} \tag{18}$$

is used regularly to measure different properties of length N vectors x. For $p = 2$ this expression is equivalent to the Euclidean norm, the limiting case for $p \to 0$ gives the number of elements not equal to zero and is called the l_0-norm

$$||x||_0 = \#\{x_i | x_i \neq 0\}, \tag{19}$$

although it is not a norm in the mathematical meaning. Nevertheless, using this definition, the l_0-norm becomes a direct measure for the sparsity of a signal.

As already mentioned in Section II, the PSFs of both the point-like and waveguide scatterers are normalized to an energy (l_2-norm) of one, leading to a dictionary with normalized atoms. With these dictionaries, an optimization problem can be formulated that minimizes the number of coefficients in α, while the error of the representation is below a certain value σ

$$\begin{aligned} &\min_{\alpha_p, \alpha_{wg}} ||\alpha_p||_0 + ||\alpha_{wg}||_0 \quad s.t. \\ &||I - \Phi_p \alpha_p - \Phi_{wg} \alpha_{wg}||_2 < \sigma. \end{aligned} \tag{20}$$

The problem stated in (20) is NP-hard and thus not efficiently solvable, but several algorithms have been proposed over the last years using either a greedy approach or a convex relaxation of the problem [17]. In this paper, a very basic greedy approach called matching pursuit [18] is used to perform the sparse decomposition and is implemented by matrix vector multiplications. In the first iteration of this algorithm, the input image is correlated with all atoms in the dictionary and the maximum correlation index is used as coefficient in α. Then the selected atom is weighted with the correlation index and subtracted from the input image, leading to the residual of the current iteration. After that, this procedure is repeated with the residual instead of the input image until a stopping criteria is met. As stopping criteria, a maximum number of iterations or the approximation error σ can be used.

IV. EXPERIMENTAL RESULTS

In this section, the decomposition result of a real ISAR image, measured by the TIRA of Fraunhofer FHR, is presented. The ISAR image of a small business jet is depicted in Fig. 2(a), the shape of the target can be seen in Fig. 2(b).

For the model, the diameter of the engine and the assumed length of the waveguide structure are needed. In the first experiment, an opening diameter of 90 cm and a length of 30 cm are used to generate the model. The length of the waveguide is approximated by the distance from the entrance to the first compressor stage. As mentioned at the end of Section II, the length of the Bessel function is important to model the damping in range. To consider this damping, the length of the Bessel function is limited to 4.5 m. This cut of the Bessel function is necessary because the model used in Section II assumes a perfectly conducting material for the waveguide. In reality the material is not a perfect conductor and the corrective term in (4) must be extended with a real exponential term that represents the damping and the decay of the artifacts in the image.

The result of the decomposition can be seen in Fig. 4 in the form of detected coordinates for the two different scattering mechanisms. The coordinates of the detected waveguide scatteres are labeled by triangles in the plots on the right side. The matching pursuit algorithm was stopped after 150 iterations and in

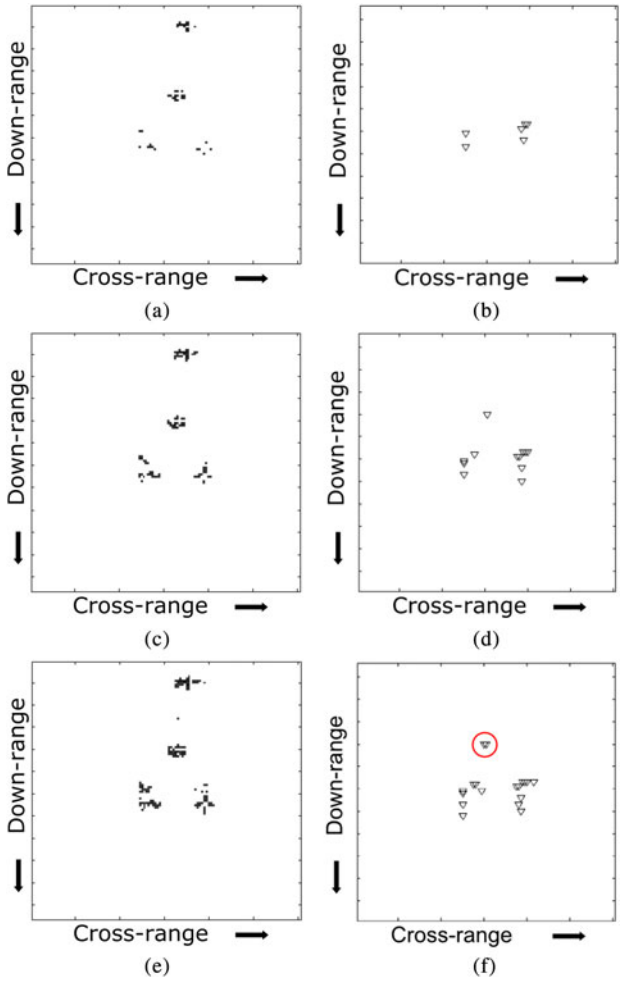

Fig. 4. Detected point-like (left) and waveguide scatterer (right). (a) 50 iterations, (b) 50 iterations, (c) 100 iterations, (d) 100 iterations, (e) 150 iterations, (f) 150 iterations.

https://doi.org/10.1017/S1759078717000757 Published online by Cambridge University Press

Fig. 4 the detected coordinates are shown after 50, 100 and 150 iterations. The last two images thus represent the final result.

In the images on the right side of Fig. 4, the detected waveguide scattering centers clearly form two pointclouds at the position of the jet engines. Two false alarms are visible in the center of the target, but with a clustering algorithm an automatic detection and location of the engines should be possible. The two false alarms are marked by a red circle in Fig. 4(f).

V. CONCLUSION AND FUTURE WORK

The sparse decomposition of ISAR images is a promising tool for feature extraction and a successful example of a model based signal processing approach. In this paper, we validated the model presented by Borden and showed a successful detection of jet engines. Nevertheless, this work can only be seen as a first step toward feature extraction via a model-based sparse decomposition; there remain many open questions and challenges for the future. One challenge is the shift from the image domain to the raw data domain, and thus incorporate the feature extraction into the imaging process. A framework that has the capability to fulfill this task was presented in [19]. Inside this framework, the mentioned damping term might be included in the model and thus give a better representation of the reality. Another open point is the use of more sophisticated algorithms to perform the sparse decomposition, like the morphological component analysis in [15].

REFERENCES

[1] Chadwick, J.; Williams, G.L.: Air target identification – concept to reality, in 2007 IET Int. Conf. on Radar Systems, October 2007, 1–5.

[2] Bieker, T.: Statistical evaluation of decision-level fusion methods for non-cooperative target identification by radar signatures, in 2008 11th Int. Conf. on Information Fusion, June 2008, 1–7.

[3] Haumtratz, T.; Worms, J.; Schiller, J.: Classification of air targets including a rejection stage for unknown targets, in 2010 11th Int. Radar Symp. (IRS), June 2010, 1–4.

[4] Rosenbach, K.; Schiller, J.: Identification of aircraft on the basis of 2-D radar images, in Radar Int. Conf., Record of the IEEE 1995, May 1995, 405–409.

[5] Chen, V.C.; Martorella, M.: Inverse Synthetic Aperture Radar Imaging, Scitech Publishing, Edison, NJ, 2014.

[6] Wagner, S.; Dommermuth, F.; Ender, J.: Detection of jet engines in ISAR images via a sparse decomposition approach for classification purposes, in 13th European Radar Conf., October 2016, 77–80.

[7] Rihaczek, A.W.; Hershkowitz, S.J.: Theory and Practice of Radar Target Identification, Artech House, Norwood, MA, 2000.

[8] Tait, P.: Automatic recognition of air targets, in H. Griffiths and D. Blacknell (eds.), Radar Automatic Target Recognition (ATR) and Non-Cooperative Target Recognition (NCTR), The Institution of Engineering and Technology, Stevenage, UK, 2013, 37–75.

[9] Ricardi, N.; Dell'Acqua, F.; Aprile, A.: JEM-line tracking in ISAR airborne radar data of flying aircrafts for engine detection, in IEEE Int. Geoscience and Remote Sensing Symp. (IGARSS), July 2015, 3175–3178.

[10] Anastassiu, H.: A review of electromagnetic scattering analysis for inlets, cavities and open ducts. IEEE Antennas Propag. Mag., **45** (6) (2003), 27–40.

[11] Borden, B.: An observation about radar imaging of re-entrant structures with implications for automatic target recognition. Inv. Probl., **13** (6) (1997), 1441–1452.

[12] Moghaddar, A.; Walton, E.K.: Time-frequency distribution analysis of scattering from waveguide cavities. IEEE Trans. Antennas Propag., **41** (5) (1993), 677–680.

[13] Orfanidis, S.J.: Electromagnetic Waves and Antennas, 2016, available online: http://www.ece.rutgers.edu/orfanidi/ewa/.

[14] Borden, B.: Radar Imaging of Airborne Targets, Institute of Physics Publishing, Bristol, UK and Philadelphia, PA, USA, 1999.

[15] Wagner, S.: Morphological component analysis in SAR images to improve the generalization of ATR systems, in 2015 3rd Int. Workshop on Compressed Sensing Theory and its Applications to Radar, Sonar and Remote Sensing (CoSeRa), June 2015, 46–50.

[16] Starck, J.L.; Elad, M.; Donoho, D.L.: Image decomposition via the combination of sparse representations and a variational approach. IEEE Trans. Image Process., **14** (10) (2005), 1570–1582.

[17] Tropp, J.A.; Wright, S.J.: Computational methods for sparse solution of linear inverse problems. Proc. IEEE, **98** (6) (2010), 948–958.

[18] Mallat, S.G.; Zhang, Z.: Matching pursuits with time-frequency-dictionaries. IEEE Trans. Signal Process., **41** (12) (1993), 3397–3415.

[19] Samadi, S.; Cetin, M.; Masnadi-Shirazi, M.A.: Multiple feature-enhanced SAR imaging using sparsity in combined dictionaries. IEEE Geosci. Remote Sens. Lett., **10** (4) (2013), 821–825.

Simon Wagner received the B.Eng. and the M.Sc. degree in Electrical Engineering from the University of Applied Sciences in Trier, Germany, in 2010 and 2013, respectively. He joined the Fraunhofer FHR in 2012 for his Master Thesis and since 2013 he is a research scientist in the NCI group of the cognitive radar department. His research interests include deep learning and sparse representation for target classification purposes. He is currently pursuing the Ph.D. degree at the University of Siegen in Germany.

Joachim Ender held the positions as the Director of the Fraunhofer-Institute for High Frequency Physics and Radar Technology FHR at Wachtberg, Germany, and as Chair for High Frequency Sensors and Radar Techniques at the University of Siegen until July 2016. After his retirement he is still active at both institutions as senior scientist. After his diploma in mathematics/physics he performed research on various topics of radar science since more than forty years. After the start of his carrier as young scientist in 1976 he became the Head of a department and in 2003 the Director of the FHR. Joachim Ender is author and co-author of numerous papers. Among other prizes, he received the "Group Technical Achievement Award – For contributions to Array Signal Processing and Multichannel Synthetic Aperture Radar" from EURASIP. In 2014, he was named as an IEEE-fellow "for contributions to multi-channel synthetic aperture radar and radar array signal processing". He was one of the founder members of the "European Conference on Synthetic Aperture Radar" (EUSAR), which takes place every two years since 1996.

https://doi.org/10.1017/S1759078717000757 Published online by Cambridge University Press